ISSN 1533-9211

DOI 10.5281/zenodo.7262709

BREAST CANCER IDENTIFICATION AND CLASSIFICATION USING FCM BASED DIVISION ALGORITHMS AND LLRBFNN

AMBIKA L G

Assistant professor, Information Science and Engineering, SJC Institute of Technology, Chickballapur, Karnataka. Email: ambikalg1991@gmail.com

Dr. T N ANITHA

Professor, Information Science and Engineering, Atria Institute of Technology, Bengaluru, Karnataka.
Email: anithareddytn72@gmail.com

Dr. JAYASUDHA K

Associate Professor, Information Science and Engineering, Atria Institute of Technology, Bengaluru, Karnataka.
Email: jayanataraja@gmail.com

Dr. MOHAMED RAFI

Professor, Computer Science and Engineering, UBDT College of Engineering, Davanagere, Karnataka.
Email: Mdrafi2km@yahoo.com

Abstract:

As indicated by the World Health Organization (WHO), bosom malignant growth conclusion is the primary driver of disease passing among ladies on the planet. Bosom malignancy happens by and large in world particularly underdevelopment and creating nations. From the clinical perspective, mammography is as yet the best symptomatic innovation, given the wide conveyance of the utilization and investigation of these pictures. The primary purpose of this article is to identify and group mammographic scars based on breast imaging site. In this work we use FCM-based computations to propose degradations for each image and compare them with the informative nearest-neighbor neural system (LLRBFNN). Characterize previous by controlling the level set rating limit, the aftermath of fluffy grouping is taken into account to further improve rendering accuracy. This methodology combines surface-highlighted images and conditions that can be used to detect and group breast malignancies. Follow-up of this study will support the best possible strategies for identifying different classes of breast disease (such as permissive or at-risk).

Keywords: Fuzzy c means, k-means, Radial basis function network, Multilayer neural network

1. INTRODUCTION

Cancer is the leading cause of unplanned death in the 2018 GC assessment total with 2.09 million deaths per year. Malignant tumors of the breast occur as a rule in women and various advances have been used. B. General Recurrent Nervous System, Multilayer Perceptron (MLP) and Stochastic Nervous System [1]. This was investigated in the Wisconsin breast disease dataset. Total recurrent nervous system and neural squad-based identification (NED) are found to be the most accurate models for characterizing breast disease [1]. Spread assumption capacity (RBF) describes the treatment of MLP options in general capacity estimation [1]. Early advances in the detection of malignant breast growth images include: X-ray, ultrasound, computed tomography (CT), induced reverberation imaging (MRI), and mammography are

The Seybold Report
ISSN 1533-9211
DOI 10.5281/zenodo.7262709

considered separately under Foundation.

Mammography is one of the current best strategies for detecting breast malignancies. It is believed to be sufficient to reduce mortality by up to 30%. Mammography has a false negative rate of 10% to 30% and a false positive rate of 10%. More than 90% of breast malignancies can be detected by mammography. Screening mammography machines are designed to detect destructive tumors early and kill them before metastases develop. Many factors affect the accuracy of mammography, including breast thickness, radiologist experience, and physical constitution. Nevertheless, an important paperwork for examining breast malignancies is the isolated deviation from the normal situation due to breast tissue differentiation [2]. This difference has limited mammography of breast tissue to mature women under the age of 40 and pregnant women who can mask the tumor. There are several methods in the literature for detecting and grouping breast diseases. Either way, there are clearly incredible tests in the detection and characterization of malignant breast cancer. Convinced of this, the further development of new computations for neighborhood direct diffusion, a premise of practical neural systems engineering, is critical for clearly recognizable evidence of bounty and intimidating detection of malignant growths in the breast. . The point of this paper is to propose a new productive framework for the characterization of breast malignancies.

DL-based picture examination has expansive applications in various fields of current drug that circuit picture data: in radiology, DL performs plenitude endeavors with human-like, or super-human, execution, for instance, tumor exposure or organ division on PC tomography (CT) pictures. Until this direct obvious toward structure, more than twelve DL systems are embraced for clinical use in radiology by the FDA—for example, DL-based assessment of CT data was done in a 2019 cell breakdown in the lungs screening trial and assertion on the clinical comfort of these procedures is quickly mounting. Drawing in resonating imaging (MRI) data, which contain commonly more information than CT data, are in like path fulfilling for DL-based mining and DL has furthermore demonstrated solid results for non-radiology endeavors, for instance, the appraisal of resolute endoscopy images and skin ailment confirmation in thermoscope images. Compared to these imaging modalities, in any case, histology is an unavoidable picture source with a striking information thickness that can be gotten from routine clinical practice. Being much more important than radiological pictures concerning pixels, pictures from histology slides pass on amazingly more information: endless different cells can be found in a histology slide, and their morphology and spatial strategy pass on all around more information than other clinical pictures.

2. RELATED WORK

The preprocessing underlying mammography prompts eliminates noise in mammography images. Sighting, segmentation, highlight extraction, highlight selection, and characterization are the kinds of modifications that rely on shape highlights to expand image complexity in both favorable and detrimental ways. Ordinary highlights, also called morphological shape features, provide a detailed representation of this class of highlights. Accuracy at various scale levels is recorded and we find that the smallest scale is twice as accurate as the largest scale. The scale

The Seybold Report
ISSN 1533-9211
DOI 10.5281/zenodo.7262709

adds extra information as computer-aided diagnosis has been proposed for clinical analysis [3].

Division of mass districts to represent surface highlights as a function of the dark surface coincident event network (GLCM) [3]. The BPNN classifier is designed to reduce the amount of false positives performed at the end of his FP part using shape checks. Use LBP in favor of most structural properties. Removed highlights should deftly distinguish between compassionate and dangerous crowds [4]. The location of malignant growth tissue is identified by screening, DWT (enhancement), thresholding (including extraction), and the order is established by the SVM classifier. It uses VIES db (75 images) and achieves 88.75% accuracy [5]. Plot the force highlights in isolation to determine volume quality. Detection using a Gabor channel (highlight extraction), histogram equalization with k-implied bunching computations using the MIAS-db dataset (upgrade) yields 99% accuracy [6]. ANN sorts objects according to the narrowest readiness test in the component space. In addition, we perform characterization using Continuous Skimming Forward (SFFS) and his PNN method as highlight selection [7]. Using tissue localization from mammography images using a neural wavelet system and placement VIES using a streamlined neural system 'PSOWNN', db achieved an accuracy of 93.67 [8-9]. The nervous system MLP [9] was simulated to determine using four biomarkers: DNA ploidy, phase fraction (SPF), and cell cycle signaling. The technique included a number of fake neural system models. Examples convolutional neural systems [10], generalized recurrent neural systems ``GRNN'' [11], probabilistic neural systems ``PNN'' [11], strong-back generative neural systems, shown in half as shown, we administered a sham neural system and the accuracy of the prepared neural system was 82.21% [12]. Yields 92.5%. In this paper, we present order-dependent splitting with FCM and AI models to demonstrate the huge size of the proposed LLRBFNN model.

Information Requested in Registers and Surveys

Personal Information		Illness History	Neoplasm information	Treatment details
Name	Address	First Date of symptoms	Diagnosis at hospital	Kind of treatment
Place of previous residence	Sex	Type of symptoms	Final diagnosis	Reason for not treatment
Date of Birth	Place of Birth	Medical advice seeking date	Site of growth	First treatment
Marital Status	Occupation	Hospital first joining date	Histology nature	Second treatment
Nationality	Parentage	Treatment started date	Stare of primary	Final treatment
Work place	Way of living in the house	Date of death/ discharge	Site of metastases	Discharge
Source of water and Food	Dietary habits	Family affected symptoms	Method of diagnosis	Recovery speed
Smoking habits	Drinking habits	Family doctor prescriptions	Family doctor advices	Maximus days for recovery
Age at the time of marriage (females)	Age at menopause (females)	Total days of illness	Final time duration	Cost of treatment

3. METHODOLOGY

Various methods have been used to study detected and classified breast cancer. This paper proposed a new method as LLRBFNN model. The resulting system was designed based on and followed the general block diagram of this procedure. A breast cancer was detected and the exact point of the scheme was shown by the new fuzzy average segmentation and classified into benign and malignant according to the next steps in the figure below.

ISSN 1533-9211

DOI 10.5281/zenodo.7262709

Fig1: Proposed Method Workflow

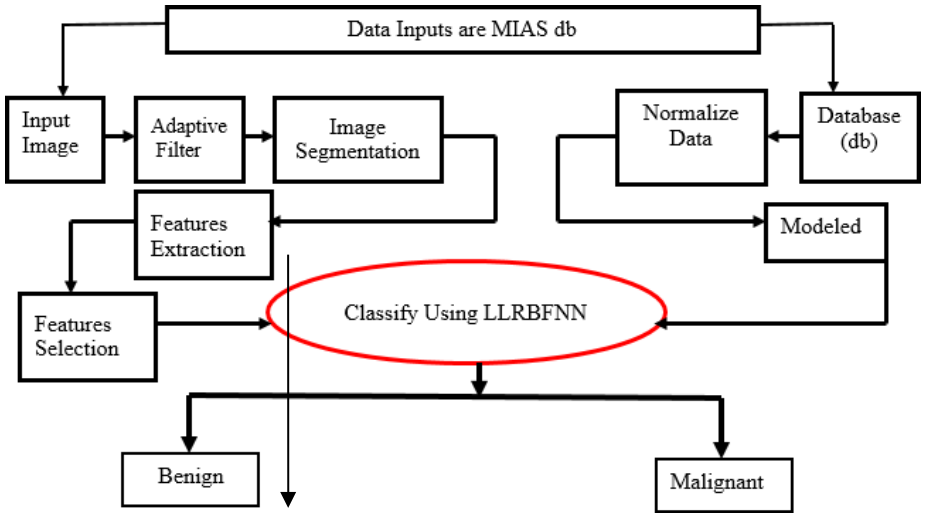

Implementation

Breast cancer detection and classification study flow chart. In the first phase, (i) the input image is segmented by his FCM technique and (ii) the GLCM technique is applied to extract features from the image. (iv)Her LLRBFNN is trained by the MWCA algorithm to detect diseases in healthy people. Indistinguishable - healthy tumor.

Fig 2: Implementation Process

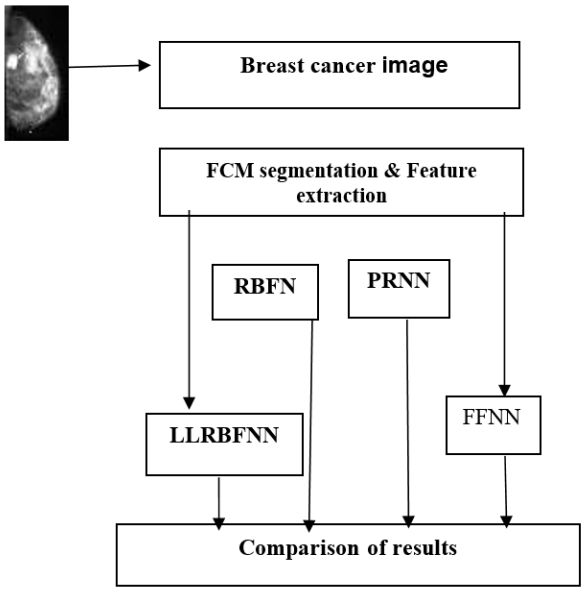

Mammogram input images were used to identify potential abnormalities and to segment areas of color images and contrast margins [13]. The system analyzes mammograms using correlated

The Seybold Report
ISSN 1533-9211
DOI 10.5281/zenodo.7262709

and uncorrelated image processing algorithms and plots histograms and scatterplots of selected variables.

GLCM (Grey Level Co-Occurrence Matrix)

Parameters like variance (var) and correlation (f) are measured for every observation and measured related variables.

$$\text{Mean}(\mu) = \frac{1}{\text{MIN}} \sum_{i=1}^{M} \sum_{j=1}^{N} P(i,j) \dots\dots\dots\dots\dots\dots (1)$$

$$\text{Standard deviation } (\delta) = \sqrt{\frac{1}{\text{MIN}} \sum_{i=1}^{M} \sum_{j=1}^{N} (P(i,j) - \mu)^2} \dots\dots\dots\dots\dots\dots (2)$$

$$\text{variance (var)} = \text{sdt}^2 \dots\dots\dots\dots\dots\dots (3)$$

$$Correlation\ (f) = \sum_{i=0}^{N_g-1} \sum_{j=0}^{N_g-1} Pd, \theta(i,j) \dots\dots\dots (4)$$

$$Contrast(f) = \sum_{n=0}^{N_g-1} n^2 \left\{ \sum_{i=0}^{N_g-1} \sum_{j=0}^{N_g-1} Pd, \theta(i,j)^2 \right\} \dots\dots\dots\dots\dots\dots (5)$$

The local measured variations of similar related contributions from P (i, j) away from the diagonal, i.e. i not equal j, then we use Kurtosis parameter to describe the shape of image a random variable's probability distribution.

$$\text{kurtosis(k)} = \left\{ \frac{1}{\text{MIN}} \sum_{i=1}^{M} \sum_{j=1}^{N} \frac{[P(i,j) - \mu]^4}{\delta} \right\} \dots\dots\dots\dots\dots (6)$$

Feature selection: In this research work, an overhead analysis (PCA) strategy was used to achieve dimensionality reduction of the VIES-DB dataset. Dimensionality reduction was a key component of our prediction demonstration. Selecting highlights reduced real-world unpredictability and improved ordering and grouping accuracy for regulated learning [14].

Filter method: We used image sifting to transform the information image into a smoothed array. Here, edge identification and de-noising limited low-power discrimination between neighboring pixels. Images were smoothed by objective edge detection and de-noising in the channel method. Two observational techniques, the direct channel and the nonlinear channel, show a straight and steady increase in activity depending on the plan, but the nonlinear task is not the most sensible choice.

Edge detection: Edge detection consists of a large number of pixels with large variations in pixel value estimates. The main idea of edge identification sieving is to determine the primary or secondary requirements of pixel value estimation.

ISSN 1533-9211

DOI 10.5281/zenodo.7262709

Expelling commotion: A smoothing channel that limits the dark contrast between adjacent pixels where subsequent images are smoothed, and a center channel that can avoid salt and pepper noise. A Gaussian channel is used to reduce the level of character agitation when the change estimate is low. The Weiner channel can significantly reduce this noise by providing a versatile center channel that can be used as a protected edge or other common part of the image.

Segmentation: A dual image was used to distinguish between dull and bright areas, making them increasingly clear. Computational separation of hues using the L*a*b* shading space. A global threshold technique and an Otsu strategy used to separate the brilliant objective elements from the weaker substrates and a fixed highest edge estimate to independently assess the distance of regions by specific boundary estimates. Projected uniformity of fragmented wounds. Where p (i,j) is the probability of a pixel having many dark planes.

$$Homogenity(H) = \sum_{i,j}^{M} \frac{P(i,j)}{1 + |i = j|} \dots\dots\dots (7)$$

$$Entropy(f) = \sum_{i=0}^{N_g-1} \sum_{j=0}^{N_g-1} Pd,\theta(i,j) loglog(Pd,\theta(i,j) \dots\dots\dots (8)$$

It is measured the variation of scenes with low first order entropy and scene high entropy that are homogeneous.

$$IDM = \sum_{i=0}^{G-1} \sum_{j=0}^{G-1} \frac{1}{1 + (i-j)^2} P(i,j) \dots\dots\dots (9)$$

$$Skewness(s) = \frac{1}{MIN} = \sum_{i=1}^{M} \sum_{j=1}^{N} \frac{(P(i,j) - \mu)^2}{\delta} \dots\dots\dots (10)$$

Root mean square level (RMS) - first non-singleton dimension calculated as below

$$\mathrm{RMS} = \frac{1}{\mathrm{N}} \sum_{\mathrm{i,j}}^{\mathrm{N}} |\mathrm{P(i,j)}^2 \dots\dots\dots (11)$$

Table 1: Statistical features of breast cancer images

Type of Parameters	Contrast	Correlation	Entropy	Homogenity	Mean	STD
Results obtained	0.4018	0.1879	4.01	0.9647	0.0026	0.0898
Type of Parameters	Variance	Smoothness	Kurtiosis	Skewness	RMS	IDM
Results obtained	0.009	0.9486	9.1762	0.8453	0.0989	1.3697

In comparison of LLRBFN [27] considered for classification task using regression function NN model

ISSN 1533-9211

DOI 10.5281/zenodo.7262709

Fig 3: LLRBFNN Architecture

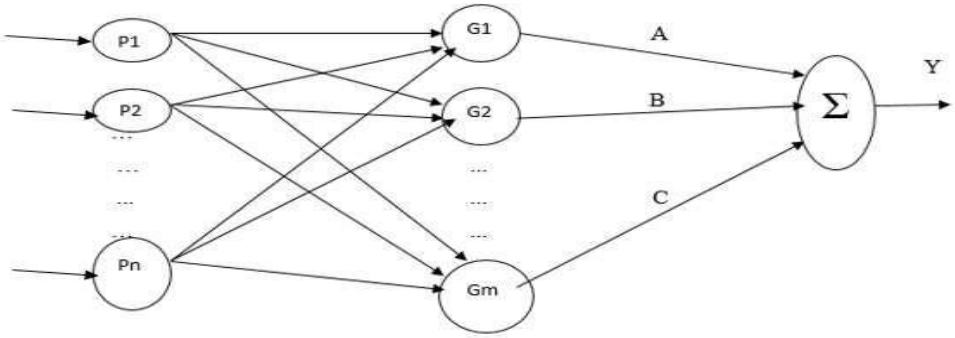

The linear equation each output node local linear given by:

$$A = W_{10} + W_{11}P1 + \cdots \ldots + W_{1npn} \quad \ldots\ldots\ldots(12)$$

$$B = W_{20} + W_{21}P1 + \cdots \ldots + W_{2npn} \quad \ldots\ldots\ldots(13)$$

$$C = W_{m0} + W_{m1}P1 + \cdots \ldots + W_{mnpn} \quad \ldots\ldots\ldots(14)$$

From the above equations variables P is input and G is activation function in the units A, B, C for given any linear equation.

The hidden layer takes the local linear weight as the input and the activation function of the M^{th} hidden neuron is defined by a Gaussian Kernel as:

$$Gm\,(p) = e^{\left(\frac{-\|p-c_m\|^2}{2\delta m^2}\right)} \ldots\ldots\ldots\ldots\ldots(15)$$

Where δm^2 the parameter for controlling the smoothness of the activation is function, cm is the center of the hidden node, the weighted linear summation in output neuron is given as:

Weight Update given for local linear network is now updated by using Widrow Hoff's Least Mean Square algorithm:

$$Wmn\,(X+1) = Wmn\;\;(X) + \eta[p]Pkn\;\;T_{km}$$

Gaussian Kernel activation given as

$$G(p) = \exp\frac{-(p-c)^2}{2\sigma^2}$$

The parameter sigma (σ) in above activation and center is taken as one .The reduced the kernel function is given below as

$$G(p) = \exp\frac{-(p-1)^2}{2}$$

Output value m^{th} unit of hidden layer is

$$Y_m = L_m G_m(L_m)$$

ISSN 1533-9211

DOI 10.5281/zenodo.7262709

$$[L_m]_{m=1}^{M} = \sum_{f=1}^{F} p_f w_{fm} = [p_1 w_{1m} + p_2 w_{2m} + \ldots\ldots\ldots + p_F w_{Fm}]_{m=1}^{M}$$

L_m Local linear weight and f = 1, 2, 3…F is number of features selections. So m^{th} hidden node output is given as

$$Y_m = \sum_{f=1}^{F} P_f w_{fm} \exp - \left(\frac{(P_f w_{fm} - 1)^2}{2} \right)$$

Thus for an input vector

$$[P_k]_{k=1}^{K} = [P_1, P_2, \ldots\ldots\ldots P_F]$$

The local linear weighted matrix is given as below

$$L = \begin{bmatrix} A \\ B \\ . \\ . \\ C \end{bmatrix}^T$$

Weight matrix L is given for matrix as

$$[L]_{1\times M} = [P]_{1\times f} \times [W]_{f\times M}$$

The output is given as

$$Y = [L]_{1\times M} \cdot\times [G]^T{}_{1\times M}$$

'G' - hidden node output is termed as below

$$\exp \frac{-(L-1)^2}{2}$$

Weight update

Widrow Hoff's Least Mean Square algorithm is used to update weight function given as below

$$w_{fm}(X+1) = w_{fm}(X) + \eta(X) P^T{}_{kf} e_{km}$$

The learning rate parameter is given as:

$$\eta(X) = \frac{\eta_0}{1 + \frac{X}{T}}$$

The LLRBFNN model compared with FFWNN, FFNN, PRNN and RBFNN for breast cancer dataset.

The Seybold Report
ISSN 1533-9211
DOI 10.5281/zenodo.7262709

4. RESULT AND DISCUSSION

Data collection

This breast cancer database was obtained from the University of Wisconsin Hospital, Madison [15]. The record contained an instance count of 400 (July 15, 1992) of 10 and a class attribute. Each instance has one of his two classes: Benign (245) or malignant. Ranking data were the ID, the 9 variables measured, and the coded class attribute. Wisconsin Breast Cancer Diagnosis (WDBC) presents nine modeled nuclear-associated variable descriptors. Collected samples were 60 benign and 100 malignant masses from the Mammography Image Analysis Association (MIAS) database request for masses and calcifications [15]. The data set collection is not normalized so that it can be read by the computer as binary, color, and grayscale images. For this reason, we prepared a normalized data set suitable for designing images that were deemed essential. Normalized record attributes ranging from zero to one (0, 1) by multiplying zero point one (0, 1) with all occurrences of the attribute except Patient ID. The final attribute class used supervised neural network learning to convert logical 0 or 1 to 1 for true and 0 for false. If the outputs are zero (0) and 1, the class is benign or malicious (1) or 0.

Simulation results for medical input image, filtered image, and segmentation image extraction functions are described separately. Returns results comparing the input medical image to the original image, true-color image, grayscale image, and histogram plot methods. Figure 4.1 shows the original image with RGB color values shown as subplots in Figure 4.1a on the left and the intensity image transformed into subplots of the same image as the heat map on the right in Figure 4.1b. Increase showed to exist.

Figure 4. 1: Dimension comparison with true color using original images

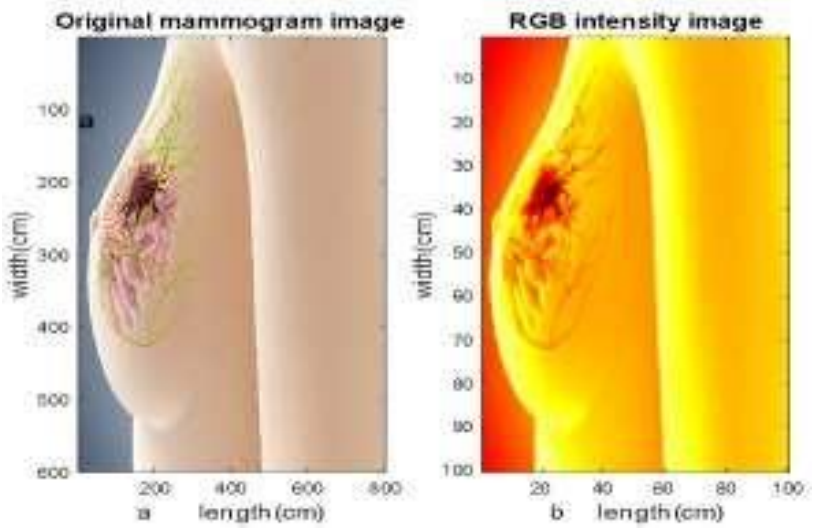

ISSN 1533-9211

DOI 10.5281/zenodo.7262709

Fig 4. 2: Comparison red color image with grayscale image analysis on histogram

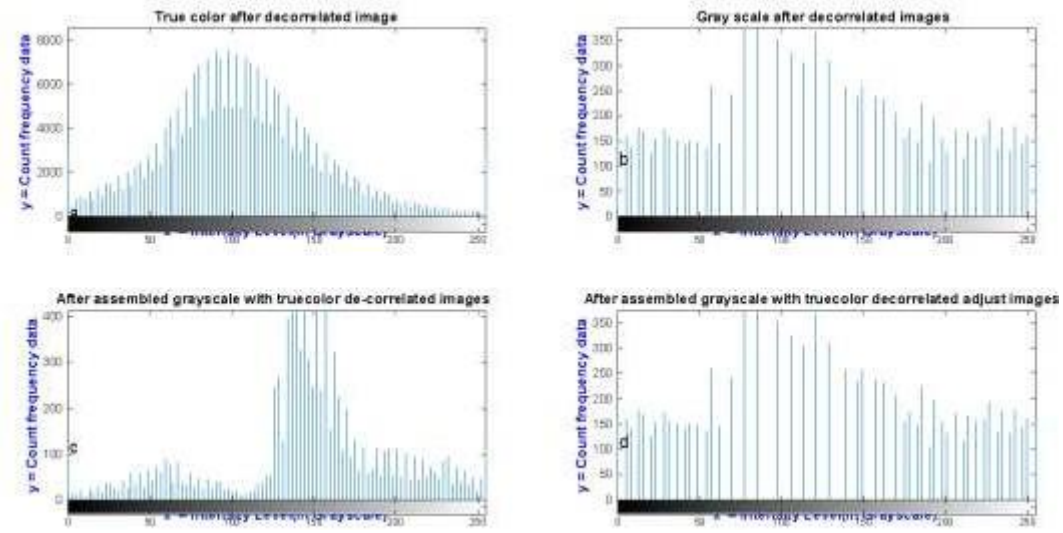

As the histogram shows, Figure 4.2b has more contrast than Figure 4.2a. The maximum value of 8000 for the count data on the y-axis was automatically reduced to 450 because the outlier peak was not dominant and its edges could be easily identified. Good separation, evaluated histogram clearly recognizable in two regions.

Noise removal results using filtering method

Mean filter, median filter and adaptive mean filter output generated using grayscale images shown below.

Fig. 4. 3: Mean filter for Noise removal and edge detection

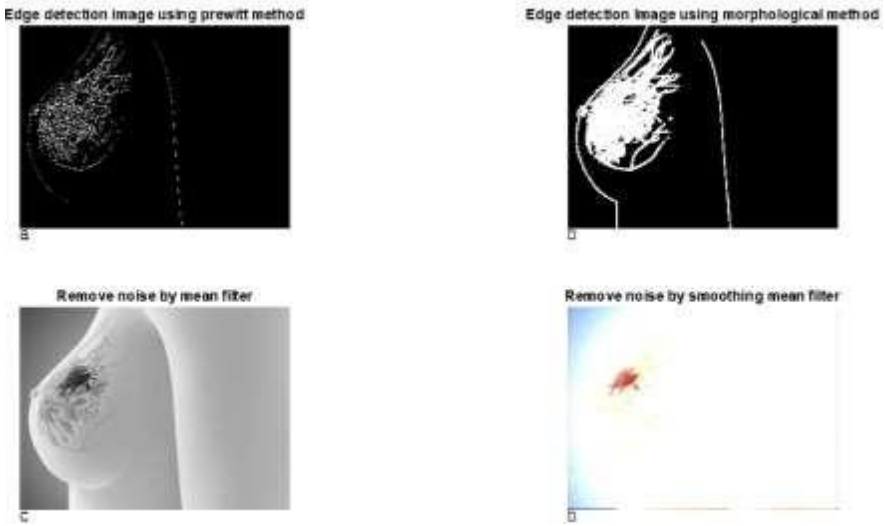

The Seybold Report
ISSN 1533-9211
DOI 10.5281/zenodo.7262709

Figure 4.3a,b shows edge detection and the remaining two show image region de-noising. Figure 4.3b shows more edge detection than Figure 4.3b. 4.3a. this was a morphological operation on a binary image. Fig. 4.3c,d, Remove the inner pixels to leave the outline of the shape, create a noise image by averaging, and display the results of the display method.

Fig. 4. 4: Remove noise and edge detection of images

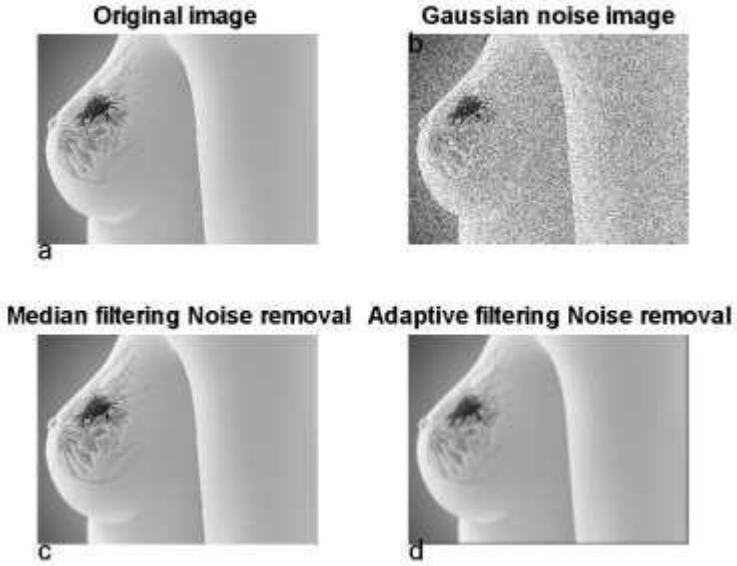

Figure 4.4a adds constant mean (0) and variance (1) noise in the intensity image as the image is de-noised with a Gaussian filter. Figure 4.4b, Adds a Gaussian image to the noisy image and displays the image in the case of a fairly large black showing only part of the image. The negative values of the Gaussian noise line were set to zero to emulate the effect of a typical detector that does not produce negative values. Figure 4.4c shows the result of filtering a noisy image with a median filter and using the medfilt2 scheme to reduce edge blurring and noise removal. Figure 4.4d was the best smoothed binary His image, de-noised using the wiener2 function scheme.

Segmentation results:

Fig. 4. 5: Segmentation of images by K-Means algorithm

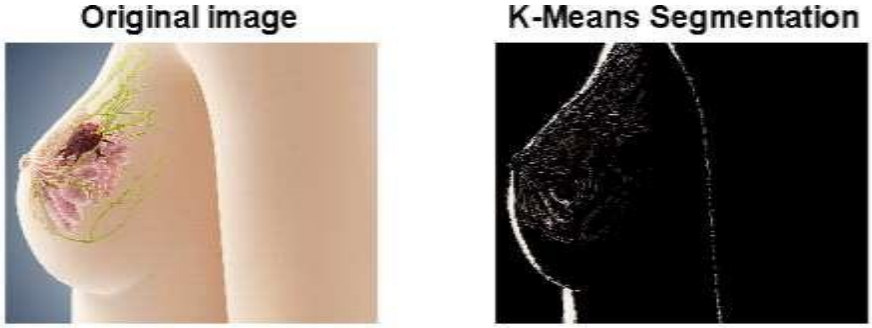

ISSN 1533-9211

DOI 10.5281/zenodo.7262709

Fig. 4. 6: Segmentation of images by En FCM algorithm

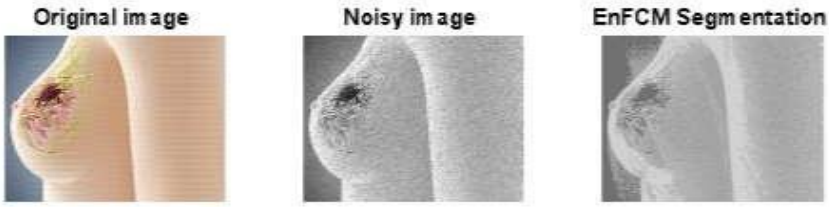

Fig. 4. 7: Segmentation of images by FGFCM algorithm

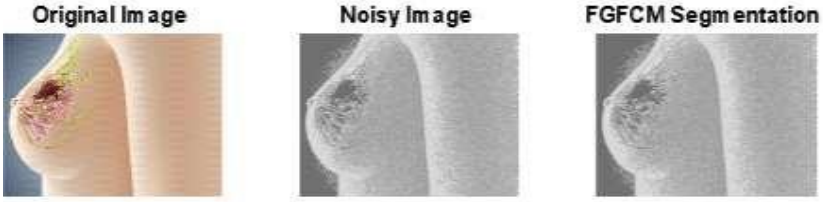

The segmentation results showed in Fig.4.5 to Fig.4.7. We observe that the FGCCM is better than EnFCM and K-Means shown in table2.

Table 2: Accuracy and Computational Time Evaluation

Algorithm type	Accuracy in%	Computational time in sec	Accuracy in%	Computational time in sec
	Special noise		Without noise	
En FCM	96.11	8.13	96.78	7.28
K-Means	97.22	**9.55**	**97.89**	**8.71**
FGFCM	98.21	5.12	**98.95**	**4.83**

Fig. 4. 8 : Mammogram images for classification

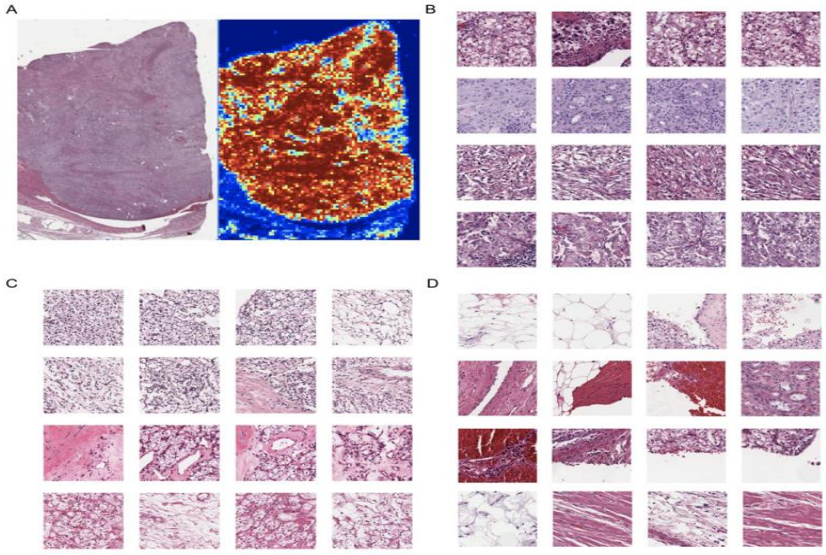

The Seybold Report
ISSN 1533-9211
DOI 10.5281/zenodo.7262709

The above Fig 4.8 shows the Mammogram images, to identify the illness and used for the survival prediction. Fig 4.11 shows the survival prediction accuracy.

4.1.2. Simulation-classification results

As shown in the following figure, the LLRBFNN output simulation results show a reduction in error. In Figure 4.9, the Y-axis represents numerical error in simulation results and the X-axis represents the number of LLRBNN iterations. The RMS performance of LLRBFNN is 0.0013 at iteration 500.

Fig. 4. 9: LLRBFNN-MSE classification

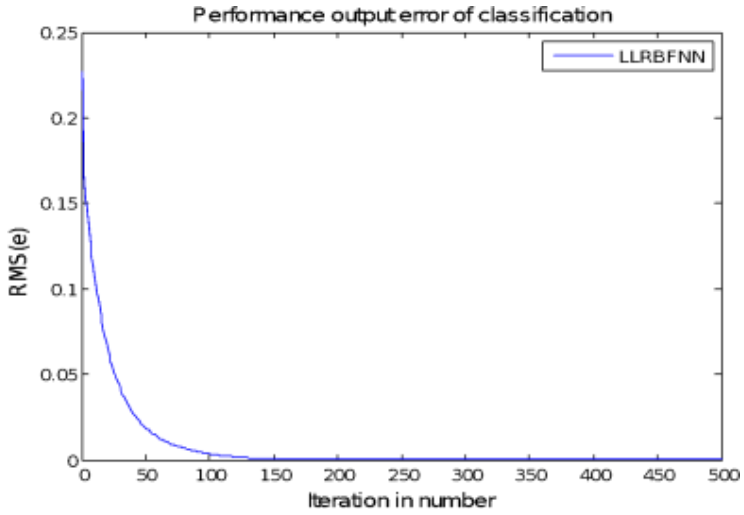

Output results for a total combination of RBFNN, FFNN, and PRNN designed for classification were obtained from MATLAB simulations and showed that the observed LLRBFNN provided particularly good classification performance.

Fig. 4. 10: MSE classification on LLRBFNN, RBFNN, PRNN, FFNN

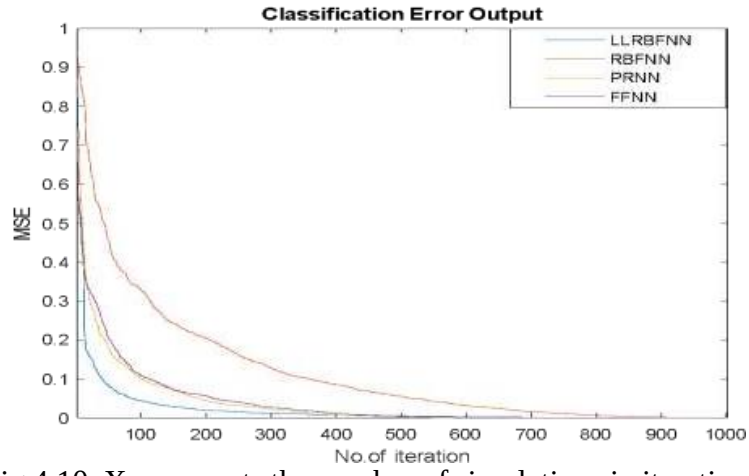

From the above Fig 4.10, X represents the number of simulations in iterations and Y represents

ISSN 1533-9211

DOI 10.5281/zenodo.7262709

the percentage of MSE. The proposed LLRBFNN plot was a blue line steadily approaching convergence at 300 iterations. The graphs were red, yellow, and magenta lines, but steadily approached convergence at 350, 600, and 850 iterations, respectively. Statistics for these parameters are shown in the table below

Table 3: Accuracy comparison

Existing Methods	Accuracy of existing methods (%)	Proposed Methods used in this research	Primary research of this paper accuracy (%) on cross validation
K-Means clustering	99%	**LLRBFNN**	99.307
Algorithm [44] SVM	95.5	**PRNN**	99.048
KNN	71.83	**FFNN**	99.048
PNN	92.5	**RBFNN**	98.33

Survival Prediction Accuracy

Fig. 4. 11: Survival probability classification

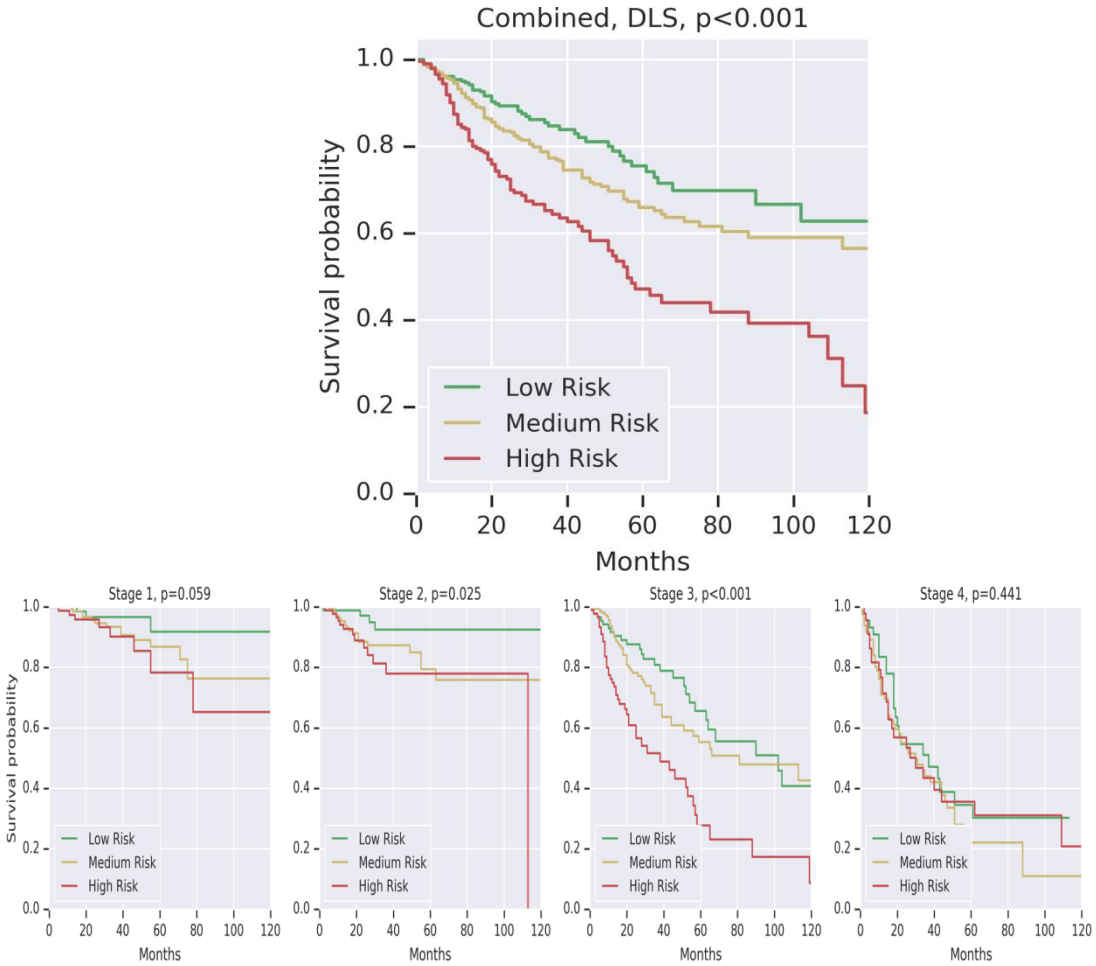

The Seybold Report
ISSN 1533-9211
DOI 10.5281/zenodo.7262709

5. CONCLUSION

Breast cancer classification is a complex and difficult task. In this study, we propose a new LLRBFNN classification model for breast cancer classification. Images are decomposed using FCM segmentation. Adaptive mean filter is used to detect breast cancer regions to get a smoother image than median filter because it preserves edges and other parts of the image. LLRBFNN was applied to unambiguously classify breast tumors based on mammogram images. LLRBFNN has been proposed to increase the accuracy of breast cancer classification as it takes good initiative at different levels of the hidden layer and may proliferate implementations of radial basis functions. Choosing appropriate parameters in a neural network is one way to improve classification accuracy. K-means clustering was also considered for classification. Minimizing the centroid distance can support clusters. If the distance between benign and malignant is non-linear, the k-mean cluster alone is difficult to separate. Therefore, to overcome this barrier of other conventional algorithms, LLRBFNN has an effective role by transforming nonlinear to linear and using k-mean clusters to split the path overhead of the two tumors. can fulfill As can be seen from the results, detection of mammogram images in Fig. and Fig. 4.4 is found to perform the smoothest and most accurate tumor detection by adaptive average filter and novel fuzzy level set method, respectively. LLRBFNN's classification design is best, among other things, to reduce errors, as shown in Figure 4.9. Future work can be done using hybrid models and soft computing applications.

REFERENCE

1. Usman Naseem;Junaid Rashid;Liaqat Ali;Jungeun Kim;Qazi Emad Ul Haq;Mazhar Javed Awan;Muhammad Imran "An Automatic Detection of Breast Cancer Diagnosis and Prognosis Based on Machine Learning Using Ensemble of Classifiers", IEEE Access 2022, Volume 10.
2. Noreen Fatima;Li Liu;Sha Hong;Haroon Ahmed "Prediction of Breast Cancer, Comparative Review of Machine Learning Techniques, and Their Analysis", IEEE Access 2020, Volume 8.
3. Ravi K. Samala;Heang-Ping Chan;Lubomir Hadjiiski;Mark A. Helvie;Caleb D. Richter;Kenny H. Cha "Breast Cancer Diagnosis in Digital Breast Tomosynthesis: Effects of Training Sample Size on Multi-Stage Transfer Learning Using Deep Neural Nets", IEEE Transactions on Medical Imaging 2019, Volume 38, Issue 3.
4. Zhiqiong Wang;Mo Li;Huaxia Wang;Hanyu Jiang;Yudong Yao;Hao Zhang;Junchang Xin "Breast Cancer Detection Using Extreme Learning Machine Based on Feature Fusion With CNN Deep Features", IEEE Access 2019, Volume 7.
5. Michiel Kallenberg;Kersten Petersen "Unsupervised Deep Learning Applied to Breast Density Segmentation and Mammographic Risk Scoring", IEEE Transactions on Medical Imaging 2016, Volume 35, Issue 5.
6. Bo Fu;Pei Liu;Jie Lin;Ling Deng;Kejia Hu;Hong Zheng "Predicting Invasive Disease-Free Survival for Early Stage Breast Cancer Patients Using Follow-Up Clinical Data", IEEE Transactions on Biomedical Engineering 2019, Volume 66, Issue 7.
7. P. Esther Jebarani;N. Umadevi;Hien Dang;Marc Pomplun "A Novel Hybrid K-Means and GMM Machine Learning Model for Breast Cancer Detection", IEEE Access 2021, Volume 9.
8. Amin Ul Haq;Jian Ping Li "Detection of Breast Cancer Through Clinical Data Using Supervised and Unsupervised Feature Selection Techniques", IEEE Access 2021, Volume 9.

The Seybold Report
ISSN 1533-9211
DOI 10.5281/zenodo.7262709

9. Abdelali Elmoufidi "Deep Multiple Instance Learning for Automatic Breast Cancer Assessment Using Digital Mammography", IEEE Transactions on Instrumentation and Measurement 2022, Volume 71.
10. Tariq Mahmood;Jianqiang Li;Yan Pei;Faheem Akhtar; "A Brief Survey on Breast Cancer Diagnostic With Deep Learning Schemes Using Multi-Image Modalities", IEEE Access 2020, Volume 8.
11. Liyang Wei;Yongyi Yang;R.M. Nishikawa;Yulei Jiang "A study on several Machine-learning methods for classification of Malignant and benign clustered microcalcifications", IEEE Transactions on Medical Imaging 2015, Volume 24, Issue 3.
12. Nishtha Hooda;Ruchika Gupta;Nidhi Rani Gupta "Prediction of Malignant Breast Cancer Cases Using Ensemble Machine Learning: A Case Study of Pesticides Prone Area", IEEE/ACM Transactions on Computational Biology and Bioinformatics, 2022, Volume 19, Issue 2.
13. Rui Hou;Yifan Peng "Anomaly Detection of Calcifications in Mammography Based on 11,000 Negative Cases", IEEE Transactions on Biomedical Engineering", 2022, Volume 69, Issue 5.
14. Zexian Huang;Daqi Chen "A Breast Cancer Diagnosis Method Based on VIM Feature Selection and Hierarchical Clustering Random Forest Algorithm", IEEE Access, 2022, Volume 10.
15. Yasin Yari;Thuy V. Nguyen;Hieu T. Nguyen " Deep Learning Applied for Histological Diagnosis of Breast Cancer", IEEE Access 2020, Volume 8.